The Coandă Drone

Design, build and control of a novel fluidically actuated drone

Eliza Argyropoulos, supervised by Dr Marko Bacic

UNIVERSITY OF OXFORD

DEPARTMENT OF ENGINEERING SCIENCE

Introduction

Background

Drones are profoundly changing the way society operates. Despite its relative infancy, the industry is already estimated to be worth $100 billion [1]. Unmanned Aerial Vehicles (UAVs) originated in the military but in future will come into direct contact with the consumer, via package delivery services, recreational vehicles, or otherwise.

Many of the drones available, particularly on the consumer market, are of n-copter configuration [2]. While a well-developed technology, the exposed moving parts will pose a safety threat to the general public as more of these vehicles take to the skies. A small number of Coandă Effect drones [3-5] have been built by others due to its improvement in efficiency, but they have mostly chosen to use flaps as a means of stabilisation. These delicate flaps on the edges of the drone are easily breakable so would not transfer well to the average consumer who is likely to crash the vehicle in the stages of learning to fly it. This project aimed to investigate the feasibility of employing a propulsion system that contains no exposed moving parts by using the Coandă Effect and ultimately looked to employ Osney lab's recently developed fluidic actuators in the design.

The Coandă Effect - The tendency of a jet to attach itself to a nearby surface [6].

Jet passes through stationary fluid and entrainment occurs. → Wall on one side diminishes stationary fluid reservoir. → Uneven entrainment leads to lower pressure area near wall, further restricting entrainment. → Equilibrium reached when jet attaches to wall.

Project Objectives

- Design and build a novel Coandă Effect drone that utilises off-the-shelf components.
- Develop a control system that makes use of conventional flap actuation to control the drone.
- Assess the thrust production and fluid flow pattern through experimentation.
- Incorporate Osney lab's newly developed fluidic actuators into the design in later iterations.

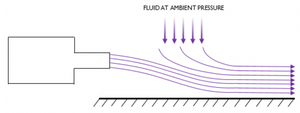

Figure 1: *Schematic Diagram of the Coandă Effect on a flat surface.*

Mechanical Design

Concept

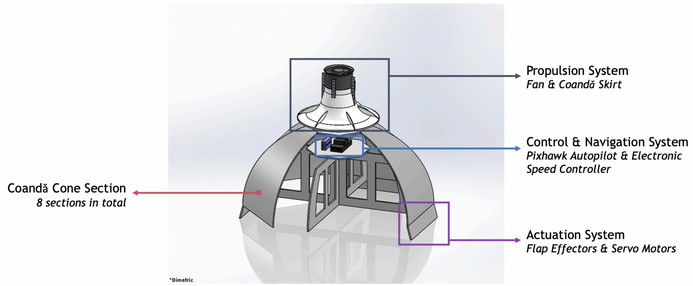

Figure 2: *SolidWorks model of the drone with key elements labelled. Two of the Coandă cone sections have been removed to display the inside of the vehicle.*

Design Selections

- **Propulsion system at the top of the Coandă cone**
  - Draws air in through a fan which is then distributed over the surface of the Coandă cone, creating a Coandă blanket that is attached to the cone surface.
- **Control Instrumentation**
  - Pixhawk 2.1 Autopilot – contains gyroscopic sensors and houses the drone's controller.
  - Electronic Speed Controller (ESC) – controls fan throttle.
  - Four servo motors – actuate the flap effectors.
  - Drone powered from the ground by 6S LiPo battery to reduce mass.
- **Flap effectors**
  - Situated on four 'control surfaces' attached to servo motors.
  - Deflect the fluid flow so the drone can be stabilised.
- **Fan skirt (3D printed)**
  - Creates duct.
  - Curved edge encourages flow to attach to the cone.
  - Gradually sloped to diffuse flow and reduce the stagnation region.
  - Circular because introducing corners to match the Coandă cone would disturb the flow.
- **Coandă cone (foam poster board)**
  - Octagonal to allow for discrete flow control.
  - Internal skeleton gives structural support to keep the shape of the cone.
  - Platform for the component shelf.
  - Ratio of the duct height and cone radius optimised so that the flow stays attached = 0.125
- **Bill of Materials**
  - Total mass of drone – 1.2 kg (measured)
  - Mass of payload and mass of structure approximately equal.

Item	Weight Cost (g)	Quantity	Total Weight (g)
Fan	309.3	1	309.3
ESC	92.7	1	92.7
Pixhawk	76.2	1	76.2
Servo Motor	8.5	4	34.0
Battery Harness	29.6	1	29.6
Skirt	105.0	1	105.0
Structural Components	553.2	-	553.2

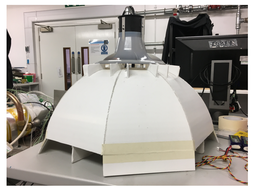

Figure 3: *Photograph of the drone taken on 31 Jan 2020. Foam board vanes inserted to ensure uniform duct height.*

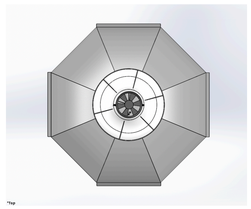

Figure 4: *Top-down view showing the octagonal Coandă cone.*

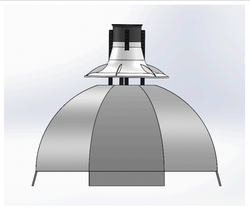

Figure 5: *Side view of the final SolidWorks model.*

Modelling

Rotor Modelling

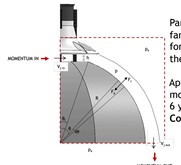

Figure 6: *Coandă jet blanket for spherical UAV momentum balance.*

Part of the flow drawn through the ducted fan is utilised for lift and part of it is used for introducing radial flow on the surface of the vehicle as a Coandă jet blanket.

Applying continuity and conservation of momentum to the control volume in Figure 6 yielded the total **lift force due to the Coandă Effect**:

$$L_{Coandă} = \frac{3}{2}\dot{m}V_{j-in}$$

- Idealised **fan thrust** derived using Actuator Disk Theory and control volume analysis
  - Assumptions:
    - Thrust uniformly distributed over rotor disk
    - Zero air swirl velocity
    - Downstream air pressure equal to undisturbed air pressure
    - Incompressible flow
    - Vehicle is in hover
  - $T = 2\rho A v_i$
    - ρ, fluid density
    - A, fan area
    - v_i, fan induced velocity
- Relationship between **fan thrust and power coefficients**, k_T and C_P respectively, derived using non-dimensional analysis equations for thrust and power from [7]
  - $k_T^3 = \frac{\pi}{2} C_P^2$

Flap Effector Modelling

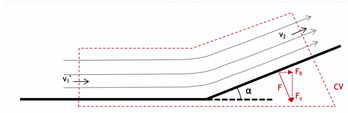

Figure 7: *Local control volume around the flap used to calculate the induced body forces.*

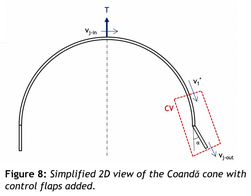

Figure 8: *Simplified 2D view of the Coandă cone with control flaps added.*

Conservation of momentum applied to the control volume in Figure 7 produced the equations for the vertical and horizontal forces induced on the vehicle by changing the flap angle, α. Comparing Figures 7 and 8 it can be seen that F_B acts vertically downwards and F_V acts towards the centre of the vehicle:

$$F_B = \dot{m}(v_1' - v_2 \cos\alpha)$$
$$F_V = \dot{m}(-v_2 \sin\alpha)$$

The forces F_B and F_V were used to establish the equations for the body forces and moments which were integrated into the system Simulink model. This model was used to design the controller that would ultimately stabilise the vehicle in hover.

General Flight Dynamics Modelling

Whilst the Covid-19 pandemic prevented the implementation of the hover controller in practice, it enabled a pivot to analysis of the dynamics of general flight for the flap-actuated drone. This provided an insight into more complicated flight modes for the drone, paving the way for a switch to fluidic actuation and ultimately enabling safer expansion of drone traffic. This modelling employs the aerospace coordinate system depicted relative to the drone in Figure 9.

Lift Force	Thrust Force	Drag Force
▪ Acts in the opposite direction to gravitational force.	▪ Acts in the direction of travel.	▪ Drone modelled as a hollow hemisphere facing the stream. ▪ Drag equation used to model the effects of drag on the drone. ▪ Opposes motion.

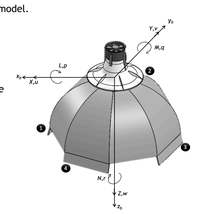

Figure 9: *Coordinate system used for the general flight equations of motion.*

Control Design

System Representation

Input nonlinear hover dynamics into Simulink. Body forces and moments were input into the Aerospace 6DoF block. → Found the steady state hover operating point and linearised about this point. Complex MIMO system created. → Simplified and decoupled into subsystems that described the φ and θ dynamics. Defined new inputs: φ subsystem input, $u_1 = \alpha_2 - \alpha_4$; θ subsystem input, $u_2 = \alpha_3 - \alpha_1$ → Augmented the two SISO subsystems with an integrator to ensure no steady state error. The subsystems to be controlled had three states each.

LQR Control

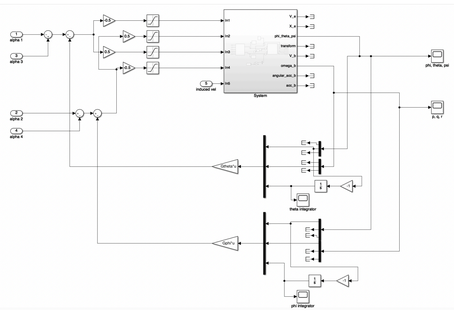

Figure 10: *Simulink model for the continuous-time simulation with LQR control implemented.*

- ✓ **Infinite Gain Margin**
- ✓ **Phase Margin > 60˚**
- ✓ **Optimal Solution**

LQR control was used to find the optimum state feedback controller, with respect to a quadratic cost function:

$$J(x,u) = \frac{1}{2}\int_0^{\infty} [x^T(t)Qx(t) + u^T(T)Ru(t)]dt$$

Q and R matrices were selected based on system behaviour and MATLAB was used to define a state feedback gain matrix, G, for each subsystem.

The two options for Q and R matrices considered were identity matrices, and those dictated by Bryson's Rule [8]. (More detail in Testing & Results section).

Figure 10 displays the Simulink model for the continuous simulation of the drone. This was used to test the behaviour of the system with different forms and magnitudes of input disturbances.

The controller was discretised with a sampling time of 0.004 s so it would be compatible with the Pixhawk Autopilot.

Unfortunately lab closure due to the pandemic prevented the controller test flights from happening.

Eliza Argyropoulos
MEng Engineering Science

eliza.argy@gmail.com
linkedin.com/in/eliza-argyropoulos/

Testing & Results

Experiments

When the first drone prototype did not fly, several experiments were carried out to investigate the amount of thrust that the fan was generating, and how much this force was diminished due to fluid flow energy losses. These experiments discovered that the drone was built based on misleading fan data – the actual fan thrust was measured to be 20.5 N, rather than the calculated 30.7 N. After reducing the mass of the vehicle and still not achieving flight, it was clear that this was not the only reason for the drone's inability to take off. Further reasons for the lack of flight were explored through fluid flow pattern experimentation.

Experiment 1: Pulley System

- Tested fan thrust by measuring the mass of water it could lift in a bucket (Figure 11).

Results

- Max fan thrust 20.5 N
- Thrust and power coefficients determined:
  - k_T = 0.621
  - c_P = 0.391
- Resulting thrust and power curves demonstrated in Figure 12.

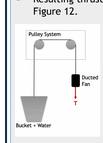

Figure 11: *Experimental apparatus.*

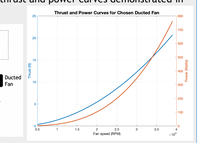

Figure 12: *Graph showing the relationship between thrust, power and fan speed.*

Experiment 2: Load Cell

- Load cell accurately measured the mass of the vehicle, and the total thrust produced by the vehicle when powered from the ground in a setting where the Coandă Effect (and losses) could be incorporated.

Results

- Drone mass excluding batteries - 1.2 kg
- Total vehicle thrust produced 5.15 N
  - Current drone design could only lift less than 50% of the vehicle's mass at 100% throttle.
  - Further drone adaptation necessary for successful flight.

Experiment 3: Duct Exit Flow Pattern

- This experiment investigated the flow distribution of the fluid at the exit of the duct created by the fan skirt. Its aim was to test whether the fan was producing a uniform jet blanket over the entire cone.
- Dynamic pressure readings taken at the top of the Coandă cone at the exit of the duct.

Results

- Flow out of the duct was non-uniform with no obvious correlation between slower flow and path blockages.
- Data shown in Figure 13 suggests that the fan generated an asymmetrical fluid flow.

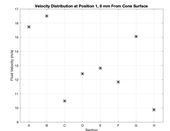

Figure 13: *Graph showing the non-uniform velocity distribution 6 mm above the Coandă cone surface at the skirt exit on each section (A-H) of the cone.*

Experiment 4: Flow Speed over Coandă Cone Section

- Dynamic pressure readings taken at six positions on Section A of the Coandă cone. Experiment was repeated for 6 mm, 12 mm, and 18 mm away from the surface.
- Experiment aim was to gain an understanding of where the Coandă jet lost contact with the surface of the cone, if at all, and to investigate whether the jet blanket dispersed into the surrounding air.

Results

- Fluid velocity reduction - Jet stream dispersed as it travelled round the cone.
- Fluid velocity at positions 5 & 6 similar - Jet widened as well as curved around the cone.
- Reduction in speed of the jet blanket was a significant factor as to why the vehicle failed to take off in its test flights.

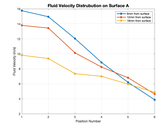

Figure 14: *Velocity distribution of the Coandă jet at three different heights above the cone surface. Much of the fluid velocity is lost as position number increases, indicating Coandă jet dispersion.*

Experiment 5: Fluid Flow Pattern Testing

i. **Ink testing:** Inconclusive as the ink was not moved by the flow.
ii. **String testing:** Demonstrated that the flow appeared to be turbulent but attached to the cone. Flow was more turbulent over the joins of the cone sections.
iii. **Smoke testing:** Smoke flow over Coandă cone showed an increase in jet blanket thickness. This confirmed the result found in Experiment 4.

Control Simulations

Q and R Matrix Selection

Identity Matrices	Bryson's Rule

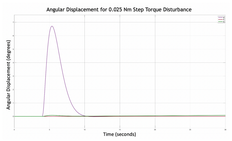

Figure 15: Stable behaviour of the drone using identity matrices for Q and R with 0.025 Nm input disturbance torque applied.

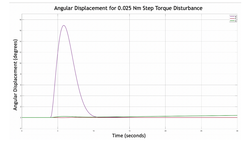

Figure 16: Simulation results for stable behaviour of the drone using Bryson's Rule Q and R matrices. Larger maximum angular displacement compared to identity matrices results.

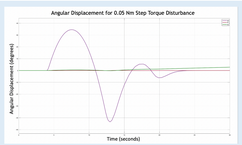

Figure 17: Drone simulation behaviour due to 0.05 Nm disturbance torque on the verge of becoming unstable.

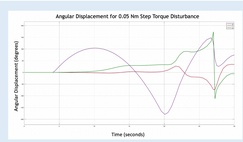

Figure 18: Drone simulation behaviour due to 0.05 Nm disturbance torque. The system is clearly unstable.

Investigation of Control Effectiveness

- System simulation could only withstand small disturbance torques of 0.05 Nm before becoming unstable. Some causes included:
  - Small mass flow rate over each cone section so each flap only had a small effect on the vehicle's orientation.
  - Maximum flap angle was 20˚ so actuator saturation was quickly reached.
- Step, pulse, and ramp disturbances tested. Figure 19 displays the maximum angular displacements before the system became unstable in each case.
  - Most favourable result for pulse disturbance – minimal displacement for small disturbances and stable for longer with larger disturbances.

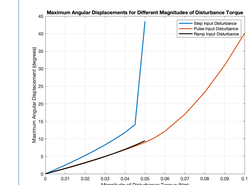

Figure 19: *Graph to compare the system's responses to step, pulse, and ramp disturbance torques.*

Project Evaluation

Achievements & Limitations

This 4YP explored the application of control methods and the Coandă Effect in a novel type of UAV both in hover and in general flight. The first version of the drone was designed, built, tested, and modified throughout the process and continuously improved. However, due to the challenges faced over the course of the project, the fluidic actuation could not be implemented. Nonetheless, this project has opened the door to further exploration into the field of UAVs with no moving parts.

Achievements

- Designed, built, and tested a Coandă Effect drone.
- Made progress into understanding the feasibility of implementing fluidic actuation in drone control.
- Learnt the necessary modifications that should be made to achieve flight.
- Additional modelling provided insight into more complicated flight modes.

Limitations

- Dissipation of the flow around the Coandă cone prevented practical implementation of the control system at an earlier stage. This meant that fluidic actuation could not be achieved in the time frame.
  - This flow dissipation also led to the small disturbance rejection.
- The practical side of the project was halted prematurely due to Covid-19 so the controller could not be tested.

References

[1] "Drones: Reporting for Work." Goldman Sachs. [Accessed May 6, 2020]. https://www. goldmansachs.com/insights/technology-driving-innovation/drones/
[2] "Consumer Drone Market Forecast 2024 - Industry Growth Report." Global Market Insights, Inc. Last modified March 21, 2018. https://www.gminsights.com/industry-analysis/consumer- drone-market.
[3] Stanton, T. "Coanda Effect Drone Propulsion." YouTube. August 16, 2019. [Accessed May 15, 2020]. https://www.youtube.com/watch?v=Irp_vnmUWZ4.
[4] Naudin, Jean-Louis. "Coanda Effect Saucer (CES) UAV with an ArduIMU+ V2." DIY Drones. Last modified December 4, 2010. https://diydrones.com/profiles/blogs/coanda-effect- saucer-ces-uav.
[5] Barlow, Chris, Darren Lewis, Stephen D. Prior, Sid Odedra, Mehmet A. Erbil, Mehmet Kara- manoglu, and Bob Collins. "(PDF) Investigating the Use of the Coanda Effect to Create Novel Unmanned Aerial Vehicles." ResearchGate. Last modified December 2009. https://www. researchgate.net/publication/228895415.
[6] Tritton, D. "Physical Fluid Dynamics Van Nostrand Reinhold", New York, Vol. 362, 1977.
[7] Spakovszky, P.Z. "Thermodynamics and Propulsion, Ch 11.7," MIT - Massachusetts Insti- tute of Technology, [Accessed 26 June 2019] https://web.mit.edu/16.unified/www/FALL/ thermodynamics/notes/notes.html
[8] Manchester, Ian R. "Course Notes." Reading, AMME4500: Guidance, Navigation, and Control, University of Sydney, June 19, 2013.